Combined analysis of the time-resolved transcriptome and proteome of plant pathogen *Xanthomonas oryzae* pv. *oryzae*

Seunghwan Kim[1], Wooyoung Eric Jang[2], Min-Sik Kim[2, 3§], Jeong-Gu Kim[1§], Lin-Woo Kang[4§]

[1]Genomics Division, National Institute of Agricultural Sciences (NAS), Rural Development Administration (RDA), Jeonju 54874, Republic of Korea; [2]Department of Applied Chemistry, Kyung Hee University, Yongin 17104, Republic of Korea; [3]Department of New Biology, DGIST, Daegu 42988, Republic of Korea; [4]Department of Biological Sciences, Konkuk University, 1 Hwayang dong, Gwangjin-gu, Seoul 05029, Republic of Korea

[§]Corresponding authors:

Dr. Lin-Woo Kang

Department of Biological Sciences, Konkuk University, Seoul 05029, Republic of Korea; Tel. 82-2-450-4090; Fax: 82-2-444-6707; E-mail: lkang@konkuk.ac.kr

Dr. Jeong-Gu Kim

Genomics Division, National Academy of Agricultural Science (NAAS), Rural Development Administration (RDA), Jeonju 54874, Republic of Korea; Tel. 82-63-238-4566; E-mail: jkim5aug@korea.kr

Dr. Min-Sik Kim, Department of New Biology, DGIST, Daegu 42988, Republic of Korea; E-mail: mkim@dgist.ac.kr

25

26 Running title: analysis of transcriptome and proteome in P-activated Xoo

27

Abstract

Xanthomonas oryzae pv. *oryzae* (Xoo) is a plant pathogen responsible for causing bacterial blight in rice. The immediate alterations in Xoo upon initial contact with rice are essential for pathogenesis. We studied time-resolved genome-wide gene expression in pathogenicity-activated Xoo cells at the transcriptome and proteome levels. The early response genes of Xoo include genes related to cell motility, inorganic ion transport, and effectors. The alteration of gene expression is initiated as early as few minutes after the initial interaction and changes with time. The time-resolved comparison of the transcriptome and proteome shows the differences between transcriptional and translational expression peaks in many genes, although the overall expression pattern of mRNAs and proteins is conserved. The discrepancy suggests an important role of translational regulation in Xoo at the early stages of pathogenesis. The gene expression analysis using time-resolved transcriptome and proteome provides unprecedented valuable information regarding Xoo pathogenesis.

Keywords: Xoo-rice interactions, proteome and transcriptome, time-resolved gene expression, *Xanthomonas oryzae* pv. *oryzae*, pathogenicity, translational regulation

Introduction

Rice (*Oryza sativa* L.) is the most widely consumed staple food, sustaining two-thirds of the world's population (Jackson, 2016). Bacterial blight of rice caused by *Xanthomonas oryzae* pv. *oryzae* (Xoo) is a devastating disease for which an effective pesticide has not been developed yet; it is known to cause severe yield losses of up to 50% in several rice-growing countries (Oliva et al., 2019). The demand for rice is expected to increase by at least 25% by 2030, owing to the rapidly growing world population, environmental stress arising in response to climate change, and pathogen pressure (Li, Wang, & Zeigler, 2014). Further, the Green Revolution has resulted in a shift in rice cultivation, from varied traditional landraces to limited high-yielding varieties, via artificial selection. This has resulted in the co-evolution of crop pathogens including Xoo with the selected host races in the modern agricultural ecosystem (Quibod et al., 2020).

The pathogen-host system of Xoo and rice serves as an ideal agricultural model to study crop diseases in a field setting at the molecular level; this is facilitated by the early elucidation of the whole genome structure of both Xoo and rice (Jackson, 2016; Lee et al., 2005). Xoo typically invades rice leaves through the wounds or hydathodes and replicates in the xylem vessels to cause disease (Mew, Alvarez, Leach, & Swings, 1993). Rice contains a two-tiered innate immune system, consisting of pathogen-associated molecular pattern- and effector-triggered immunity, which protects against Xoo and initiates the hypersensitivity response at the infection site (Jones & Dangl, 2006). In Xoo-rice interactions, Xoo injects effectors into rice cells to modulate the cellular activities of the host to promote pathogenesis (Tsuge, Furutani, & Ikawa, 2014). The early interactions between Xoo and rice at the infection site determine the fate of infection, i.e., occurrence of disease or initiation of the immune response. The environmental conditions prevalent at the site of infection are varied and complex, and our

69 understanding of alterations in the Xoo cells in response to the initial interactions with rice is
70 limited.

71 Transcription and translation are tightly coupled in bacteria and can occur simultaneously in
72 the cytosol (Hershey, Sonenberg, & Mathews, 2019). Although proteins are the final functional
73 products of genes, the quantity of specific mRNA molecules often represents the expression
74 level of a gene at a given time point with the well-established RNA sequencing (RNA-Seq)
75 technology. In comparison, high resolution mass spectrometry-based quantitative proteomics
76 is a more recent analytical technique, and still has a lower coverage of protein products,
77 requires greater sample quantity, and is more expensive (Schubert, Rost, Collins, Rosenberger,
78 & Aebersold, 2017).

79 We had previously developed an *in vitro* pathogenicity assay to recapitulate Xoo-rice
80 interactions at the site of infection by treating Xoo cells with the rice homogenate (RLX), and
81 assessed the time-resolved changes in the transcriptome (S. Kim et al., 2016; S. H. Kim et al.,
82 2011; S. Kim et al., 2013). The *in vitro* pathogenicity assay provides high signal to noise data
83 with Xoo cells synchronized with respect to the timing of pathogenicity activation.
84 Transcriptome data from RNA-Seq experiments revealed that most virulence genes of Xoo
85 were upregulated within an hour of the initial interaction with RLX, and these upregulated
86 genes were related to bacterial motility, inorganic ion transport, hypersensitive response and
87 pathogenicity (*hrp*), bacterial toxins and effectors of avirulence (*avr*), plant cell wall
88 degradation, and extracellular polysaccharide synthesis and secretion (S. Kim et al., 2016).

89 Here, we expand the study of gene expression in pathogenicity-activated (P-activated) Xoo
90 from the transcriptome to the proteome. The time-dependent expression of specific mRNAs
91 and proteins represents the kinetics of transcriptional and translational expression of certain
92 genes and allow the visualization of the immediate alterations in gene expression in P-activated

Xoo.

95 **Results**

96 **Time-resolved proteome data**

97 We coupled LC-MS/MS technology with an *in vitro* assay system to obtain the time-resolved
98 proteome data for P-activated Xoo cells (Scheme 1). The *in vitro* assay system recapitulated
99 the initial interaction between Xoo cells and damaged rice leaf tissues at the site of infection;
100 this was achieved by adding fresh RLX—prepared by grinding the leaves of a Xoo-susceptible
101 rice cultivar (Milyang 23) in liquid nitrogen—to a Xoo cell culture in the mid-exponential
102 phase. Samples for proteome analysis were collected from RLX-treated (P-activated) and
103 untreated (control) Xoo cells at 0, 30, 60, 90, and 120 min after RLX treatment (Table S1).

104 Analysis on UniProt revealed that the total 4,956 predicted open reading frames in the Xoo
105 genome (KACC10331) corresponded to 4,382 proteins in the proteome, of which 2,589
106 proteins (59%) were identified for at least one time point and 2,296 proteins (52%) were
107 detected in both replicates (Figure S1A). Median sequence coverages for total identified
108 proteins were 24% and 23% for each of the independent duplicate experiments (Figure S1B).
109 A total of 20,963 and 19,684 non-redundant peptides were identified in both replicates, with
110 47,025 and 41,428 peptide-spectrum matches, respectively (Figure S1C).

111 Protein abundance values obtained after quantile-normalization (Figure S2A) were used for
112 pairwise comparisons; the Pearson's correlation coefficients corresponding to the abundance
113 values showed close correlations (0.98-0.99), indicating comparable cellular concentration of
114 most proteins (Figure S2B). The smallest correlations were observed for the RLX-treated
115 samples at 30 min, indicating greater changes in the proteome during the initial 30 min; this
116 was consistent with the transcriptome data. We further performed a principal component
117 analysis to determine the relationships between the assessed samples. Figure S2C shows that
118 the P-activated sample at 0 min clustered closely with all control samples, whereas the P-

activated samples at other time points were more spread out. The proteome of the P-activated Xoo cells at 30 min was considerably different from that of P-activated Xoo at other time points; this was consistent with the results of the pairwise multi-scatter plot (Figure S2B).

Time-supervised hierarchical clustering was performed to determine temporal and synchronized changes in protein abundance. Two distinct synchronized patterns—one decreasing and the other increasing in response to RLX treatment—were observed (Figure 1). The two lists including proteins exhibiting the two patterns were used for STRING analysis, which produced two interaction networks (Figure S3A-B). Several genes related to cell motility, inorganic ion transport, and transcriptional regulators were immediately responsive to the pathogenicity signal (Table S2); these have been described in detail in the discussion section.

Up and down regulated proteins

Quantitative proteome data obtained from P-activated and control Xoo cells at every 30 min allowed the visualization of the three-dimensional protein expression data in terms of the genes, time intervals, and expression levels (Figure 2 and Table S3). The expressed protein level of each gene from P-activated Xoo cells are divided by that of the same gene from control at each time point to calculate the fold change of time-dependent protein expression level of the specific gene. For all the open reading frames, approximately 93 (2.0%), 213 (4.5%), and 468 (9.9%) proteins were upregulated by more than 200% (2-fold), 50%, and 20% at 30 min, respectively, and approximately 7 (0.1%), 93 (2.0%), and 561 (11.9%) proteins were downregulated to less than 25% (2-fold), 50%, and 80% at 30 min, respectively (Table S4).

In case of the duration of expressed proteins in P-activated Xoo, only 8 (0.2%), 32 (0.7%), and 75 (1.6%) proteins were upregulated for entire 120 min by more than 200% (2-fold), 50%, and 20%, respectively and 0 (0%), 1 (0.02%), and 87 (1.8%) proteins were downregulated for

143 the same 120 min to less than 25% (2-fold), 50%, and 80% , respectively (Table S5), indicating
144 that most proteins were temporarily up- or downregulated in the *in vitro* assay.
145 The proteins at 30 min presented the highest change at the expression level within 120 min.
146 More than 90 proteins (1.9%) were upregulated by more than 2-fold at 30 min in each dataset,
147 whereas 27 proteins were upregulated in both datasets from the duplicate experiments (Table
148 S6). Almost half of the 27 upregulated proteins were related to cell motility and ion uptake,
149 seven were related to chemotaxis and motility, and five were related to transporters and pumps.
150 At the same 30 min, more than 90 proteins were downregulated by more than 50%, 17 proteins
151 were downregulated in both datasets (Table S7), including transcription-related proteins—such
152 as sigma-54 modulation protein and MetE/MetH family transcriptional regulator—and cell
153 division- and cell cycle-related proteins.
154
155 **Clusters of Orthologous Groups of proteins (COGs)**
156 To study the global gene expression pattern based on gene function, we superimposed time-
157 dependent protein expression levels as per the functional categories in the Clusters of
158 Orthologous Groups of proteins (COGs) database (Figure 2), which were grouped into three
159 classes (red, yellow, and blue) depending on the observed pattern. To facilitate the comparison
160 of time-dependent protein expression levels, the expression level at 0 min was set as the
161 reference level (=1) for each gene, and the fold change in the protein expression level was
162 calculated at each time point, as in case of the RNA-Seq data analysis (S. Kim et al., 2016).
163 The most prominent changes in protein expression in Xoo cells were observed for proteins
164 associated with cell motility (N) and inorganic ion transport and metabolism (P), which were
165 placed in the red class. In category N, two major expression peaks, indicating more than 2-fold
166 up-regulation, were detected at 30 and 90 min. In category P, upregulated proteins peaked at

167 around 30 min. Proteins grouped in the yellow class exhibited moderate changes in their
168 expression level, and were divided into nine functional categories, including signal
169 transduction (T), intracellular trafficking, secretion, and vesicular transport (U), energy
170 production and conversion (C), transcription (K), replication (L), cell wall/membrane/envelop
171 biogenesis (M), and protein turnover (O). The blue class included proteins associated with other
172 nine categories, the expression levels of which exhibited little change when compared with
173 those at 0 min, albeit except for a few proteins.
174
175 **Comparison of mRNA and protein levels**
176 We compared mRNA and protein levels of each gene in the transcriptome and proteome
177 (Figure 3; thin dashed red lines of mRNAs and thick dashed and solid black lines of proteins).
178 Both transcriptome and proteome data were obtained for up to 120 min after RLX treatment.
179 The experimental procedure used to prepare protein samples for LS-MS/MS required at least
180 30 min, whereas that for mRNA samples required at least 5 min; the time interval for the
181 proteome data was set to 30 min, whereas that for transcriptome data was set to 5-30 min. Due
182 to the different sampling times, the transcriptome data included mRNA levels at additional time
183 points of 5, 10, 15, and 45 min, whereas the proteome data did not include protein levels
184 between 0 and 30 min, in which case the protein levels (thick dashed black lines) were
185 extrapolated based on the protein levels at other time points using non-linear regression.
186
187 *Flagella and chemotaxis-related genes*
188 Flagella and chemotaxis-related genes encode more than 40 proteins, including structural
189 components and assembly factors of flagellar hook-basal body and filament and chemotaxis
190 proteins (Mukherjee & Kearns, 2014). Two dominant hierarchical clusters, with distinct

191 synchronized patterns of increasing and decreasing proteome concentration (indicated by red
192 and blue, respectively), were identified (Figure 1). The red cluster of 359 proteins included 21
193 (53%) of the 40 genes related to the flagellar assembly pathway, of which 20 genes were
194 included in the red cluster (Table S2).

195 We grouped the flagella and chemotaxis-related genes into three gene clusters, i.e., groups
196 I-A, I-B, and II, based on their positions in the genome (Figure 4A). Genes in cluster I-A and
197 I-B were associated with flagellar machinery, such as flagellar basal body hook and type III
198 secretion system (T3SS), whereas cluster II included chemotaxis-related genes.

199 Superimposition of transcriptome and proteome data of cell motility related genes revealed
200 clearly superimposed upregulated peaks at 30 min (Figure 3A). The transcriptome data
201 revealed that most flagella and chemotaxis-related genes were regulated in a similar pattern,
202 i.e., genes in all clusters of I-A, I-B, and II were downregulated at 5 min and upregulated at 30
203 min. However, the proteome data presented a different expression pattern between clusters I-A
204 and I-B and cluster II. Proteins in clusters I-A and I-B were upregulated at 30 min, consistent
205 with the transcriptome data. But proteins in cluster II were upregulated at 90 min, exhibiting a
206 delay of 1 h when compared with the transcriptome data (Figure S4).

207

208 *Inorganic ion transport and metabolism genes*

209 Iron uptake genes play a key role in pathogenicity during the early stages of host-pathogen
210 interactions (Garau et al., 2004). TonB-dependent receptors (TBDRs) are bacterial outer
211 membrane proteins that bind and transport ferric chelates of siderophores. Several annotated
212 TBDR genes have been identified in the Xoo KACC10331 genome, including *IroN*, *FyuA*,
213 *FecA*, *BtuB*, *FhuA*, *CirA*, and *FepA* (S. Kim et al., 2016). Of these, *FecA* (*Xoo0901*) and *CirA*
214 (*Xoo3793*) were upregulated and *IroN* genes (*Xoo0394* and *Xoo1784*) were downregulated in

215 both the transcriptome and proteome data. In the proteome data, *FecA* (*Xoo0901*) and *CirA*
216 (*Xoo3793*) upregulation peaked at 30 min (Figure 5A). *IroN* genes that were downregulated at
217 the transcript level were also downregulated at the protein level (Figure 5B). The expression
218 levels of other paralogs of *FecA* and *CirA* genes were comparable with those in the control in
219 the transcriptome as well as the proteome data (Figure S5), indicating that these genes could
220 respond to different pathogenic signals—which were missing in the *in vitro* system—or be
221 pseudogenes.

222 Phosphate uptake genes, i.e., *OprO*, *PhoX*, *PstSCAB*, and *PhoU*, were upregulated in the
223 transcriptome (up to 16-fold) at 5-10 min. The proteome data of OprO, PhoX, PstSCAB, and
224 PhoU revealed upregulation up to 3-fold at 30 min (Figure S6).

225

226 *Expression and secretion of effectors*

227 In *Xanthomonas oryzae* pv. *oryzicola*, AvrBs2 suppresses host immunity and promotes
228 disease development (Ullah et al., 1998). In *Xanthomonas campestris* pv. *vesicatoria*, the role
229 of AvrBs3 is that of a transcription activator-like (TAL) effector that activates the expression
230 of plant immunity genes (Kay, Hahn, Marois, Wieduwild, & Bonas, 2009). The secretion of
231 effectors XoAvrBs2 (*Xoo0168*)—a Xoo ortholog of AvrBs2—and XoAvrBs3 (*Xoo2276*)—a
232 Xoo ortholog of AvrBs3—through T3SS was confirmed upon interaction with RLX (S. H. Kim
233 et al., 2011; S. Kim et al., 2013). In addition to the transcriptome and proteome, the expression
234 and secretion of effectors were assessed using dot blots of Xoo cells transformed with the TAP-
235 tagged effector genes (Figure 6).

236 The expression of *XoAvrBs2* transcript was upregulated from 5-30 min, while that of the
237 XoAvrBs2 protein was upregulated at 30 min, as is evident from the transcriptome and
238 proteome data. In the dot blots, the levels of TAP-tagged XoAvrBs2 were upregulated by 4-

239 fold at 5 min and the secretion of XoAvrBs2 was detected as early as 15 min. The expression
240 of *XoAvrBs3* transcript was upregulated and peaked from 5-30 min, whereas that of XoAvrBs3
241 protein was maintained at almost the same—or slightly lower levels—at 60 min in the
242 transcriptome and proteome data. Dot blots revealed the secretion of XoAvrBs3 from 15 min.
243

244 **Discussion**

245 Plant pathogens could exhibit complex responses to the initial interactions with the host
246 under varying biotic and abiotic conditions at the site of infection. The varied immediate
247 response of the plant pathogen is important for successful infection. In this study, we analyzed
248 the immediate time-resolved response of Xoo cells from the initial interaction with rice in terms
249 of gene expression at both the mRNA and protein levels using an *in vitro* assay system, wherein
250 RLX mimicked the damaged rice leaf tissue (Scheme 1).

251 Of all the predicted open reading frames in Xoo, we quantified approximately 83% and 47%
252 of the mRNAs and proteins, respectively, in a time-dependent manner. A good correspondence
253 of overall expression pattern was observed between the mRNA and protein levels of genes. The
254 expression pattern was more synchronized for genes closely located in the genome (Figure 4
255 and S4); this could be attributed to the polycistronic gene structure in bacteria. With respect to
256 the rapidity of pathogenic gene expression in response to the signals triggered upon interaction
257 with the host, both transcriptional and translational machineries responded immediately to the
258 interaction, at the earliest assessed time points of 5 and 30 min in the transcriptome and
259 proteome data. The secretion of effectors was also found at 15 min in dot blots. Both mRNAs
260 and proteins presented the greatest variation in their levels during the initial 30 min.

261 The Xoo genes exhibiting the most rapid responses to the initial interaction with RLX,
262 included genes associated with cell motility and inorganic ion uptake, and genes coding for
263 effector molecules. All these three functional categories of genes are closely related to the early
264 stages of pathogenesis. The genes associated with cell motility could be responsible for the
265 migration and accumulation of the Xoo cells at the site of infection via the damaged xylem
266 tissues or exposed hydathodes in rice. As inorganic ions, such as iron and phosphate ions,
267 function as essential cofactors in all living organisms, bacterial pathogens and host rice cells

268 compete to obtain and secure the limited resources available. Effector molecules are more
269 directly related to pathogenesis and are injected by the Xoo into the rice cells via pili-like T3SS;
270 these molecules modulate the immune system of rice.

271 The earliest available time-point for comparing the gene expressions in terms of mRNA and
272 protein levels was 30 min after the RLX treatment. At 30 min, 290 mRNAs were upregulated
273 by more than 2-fold in the transcriptome, compared with 93 proteins in the proteome (Table
274 S4), and the average fold change in the expression of the upregulated genes in the transcriptome
275 and proteome was similar, i.e., 3.3-fold and 3.4-fold, respectively (Table S6). The number of
276 upregulated transcripts is much higher than—even though we figure into our calculations the
277 higher coverage of quantified genes in transcriptome than in proteome—that of the proteins at
278 30 min, which indicates that not all the upregulated mRNAs are simultaneously translated to
279 proteins.

280 The difference in the gene expression in terms of the mRNA and protein levels at a given
281 time point suggests the existence of an additional translational regulation step—after the
282 transcriptional regulation—although transcription and translation can occur simultaneously in
283 bacteria. For some genes, the mRNA and protein expression peaks were observed at varying
284 time points. Bacterial pathogenesis appears to involve a fine-tuning mechanism after
285 transcription, which could help adjust the expression of the early-responsive genes under
286 varying biotic and abiotic environmental conditions.

287 Genes related to flagella and cell motility are clustered in the bacterial genome. In Xoo, three
288 clusters are observed, i.e., I-A, I-B, and II. On superimposing the mRNA and protein levels in
289 time, the expression of mRNAs and proteins peaked at 30 mins for genes in the clusters I-A
290 and I-B, the expression of mRNAs and proteins peaked at 30 and 90 min, respectively, for
291 genes in cluster II. A translational regulation step might be involved that determines the time

292 for the translation of specific mRNAs—coded by flagella and cell motility-related genes—into
293 proteins depending on the priority of each gene.

294 The hierarchy of the expression of flagella and cell motility-related genes has been
295 extensively studied in the transcriptome of *E. coli*, where sigma and anti-sigma factors are
296 known to be the key transcriptional regulators (Mukherjee & Kearns, 2014). The overall
297 organization of flagella and chemotaxis-related genes is different between *E. coli* and Xoo
298 (Figure S7). In Xoo, the cluster of *fliE-R* genes (cluster I-B) is positioned just downstream to
299 the *flgB-L* genes (cluster I-A), whereas in *E. coli,* chemotaxis genes are present between the
300 two. *flhDC* genes do not have any orthologs in Xoo, and a different transcriptional regulator,
301 i.e., the *fleQ* gene, is present. Based on the nomenclature used in *E. coli*, several Xoo genes
302 classified as Class III genes are located at different positions and their expression regulation is
303 also different. In Xoo, ribosomes or other translation factors might recognize certain unknown
304 priority signals in mRNA transcripts for the translational regulation.

305 The immediate upregulation of inorganic ion uptake genes, especially iron uptake genes,
306 may aid Xoo cells to obtain the essential cofactor ions, when they are competition with the host
307 cells (Liu, Kong, Wu, & Ling, 2020). The iron ion is essential for photosynthesis and respiration
308 and needed by many redox enzymes for most organisms on Earth. Pathogens commonly use
309 iron chelating molecules or siderophores to derive this scarce inorganic cofactor from the hosts.
310 The leakage of iron ions from damaged leaf tissues might serve as an important signal of
311 initiating infection and might provide an opportunity to secure essential iron ions for the Xoo
312 cells.

313 In comparison with the flagella and cell motility-related genes that are closely clustered in
314 the genome and exhibit coordinated expression levels, the ion uptake genes are dispersed across
315 the genome and are independently expressed (Figure S8). The separation of these genes

316 facilitates independent regulation. Compared with the flagella and motility-related genes, the
317 inorganic ion uptake genes exhibited great variation in the mRNA levels but similar protein
318 expression levels (Figure 3).

319 Effectors are key molecules for pathogenicity that modulate the host immune responses after
320 infection. The protein expression and secretion of the Xoo effectors XoAvrBs2 and XoAvrBs3
321 were assessed using dot blots, which enabled the monitoring of effector proteins at the early
322 stages of the initial interaction, i.e., within 30 min of RLX treatment. The secretion of effectors
323 was observed from 15 min after application of the pathogenic stimulus. In the P-activated
324 proteome data, the expression of effector proteins was maintained at a similar level to that at 0
325 min; this may be attributed to the similar protein synthesis and secretion rates.

326 The effector genes are also dispersed across the genome, like the ion uptake genes (Figure
327 S9). Interestingly, transposase genes are located close to the effector genes; these may aid the
328 effector genes to transpose through the bacterial genome and plasmids. The expression of
329 XoAvrBs2 was upregulated 5 min after RLX treatment, and its secretion was detected in the
330 culture medium at 15 min. Although the cellular protein level was upregulated by
331 approximately 20% in the proteome at 30 min, the dot blot showed an upregulation of 4-fold
332 at 5 min. The secreted XoAvrBs2 exhibited a 16-fold increase at 120 min. In case of XoAvrBs3,
333 the cellular protein level decreased by approximately 20% in the proteome at 60 min, whereas
334 the dot blot revealed a 16-fold increase in XoAvrBs3 secretion at 120 min. The experimental
335 methods for proteome and dot blots analysis are different (S. H. Kim et al., 2011; S. Kim et al.,
336 2013). For the dot blots analysis, TAP-tagged *XoAvrBs2* and *XoAvrBs3* genes were introduced
337 into Xoo cells via the plasmid having the endogenous promotor and expressed from the plasmid.
338 In the proteome analysis, XoAvrBs2 and XoAvrBs3 proteins were expressed from the
339 endogenous *XoAvrBs2* and *XoAvrBs3* genes in the Xoo genome.

340 Gene expression involves sequential transcription and translation. In bacteria, with respect
341 to post-transcriptional and post-translational modification, mRNAs without a cap at 5' end and
342 a poly A tail at 3' end have a short half-life—as short as few minutes—and proteins undergo
343 only limited post-translational modifications. The limited post-translational modifications in
344 bacterial proteins impose a pressure on a nascent protein from the ribosome to take a functional
345 form immediately. The present study revealed that genes related to cell motility and inorganic
346 ion uptake, and genes coding for effector molecules of Xoo are the first to respond to the initial
347 interactions with RLX, and play an essential role in the following processes (Figure 7): (1)
348 invasion of the Xoo cells into the rice leaf tissues, (2) securing the limited cofactors, and (3)
349 modulating the immune responses of the host to favor pathogenesis. This combined analysis of
350 the time-resolved transcriptome and proteome of Xoo during the initial interaction with rice
351 tissues provides valuable insights into the pathogenic mechanism of Xoo.
352

353 **Materials and Methods**

354 **Bacterial strain and culture conditions**

355 *Xanthomonas oryzae* pv. *oryzae* (Xoo) strain KACC10331, consisting of 4,941,439
356 nucleotides and 4,733 open reading frames, without any apparent autonomous plasmids, was
357 obtained from the Korean Agricultural Collection Center (KACC) (Lee et al., 2005). The
358 bacteria were cultured in nutrient broth (Difco, Detroit, MI, USA) or Yeast Glucose Cm Agar
359 (YGC) (1% yeast extract, 2% D-(+)-glucose, 2% $CaCO_3$, and 1.5% agar) at 28°C.

360

361 **Construction of expression vector and transformation of Xoo**

362 The effector genes *XoAvrBs2* (*Xoo0168*) and *XoAvrBs3*—including the promoter region
363 (from -149 and -750 bp to the start codon of the respective gene)—were amplified by PCR and
364 ligated into the pGEM®-T Easy Vector (Promega). The cloned sequences were verified and
365 then digested with *Kpn*I and *Sac*I, and the products were ligated into the pHM1-XTAP-T_{gap}
366 vector. The recombinant vectors were purified and introduced into Xoo strain KACC10331 by
367 electroporation, using Gene Pulser II (Bio-Rad, Hercules, CA) with a 0.2 cm-gap cuvette at 2.5
368 kV cm^{-1}. Xoo cells were then diluted immediately with 1 mL Super Optimal Broth (SOC)
369 medium and incubated at 28°C with agitation for 2 h. Cells were then recovered from the
370 culture medium and plated on nutrient broth agar plates containing 50 μL mL^{-1} spectinomycin
371 and incubated at 28°C for 4 d.

372 The transformants were cultured in 100 mL of nutrient broth up to the mid-exponential
373 phase (A_{600} = 0.5). Cells were harvested by centrifuging 1 mL of the cell culture at 12,000 rpm
374 and 4°C for 5 min. Harvested cells were washed once with phosphate-buffered saline (PBS) at
375 pH 7.2, resuspended in 200 μL PBS, and then sonicated. Protein samples were serially diluted
376 using 2 M urea in PBS in 96-well plates and then transferred to a polyvinylidene difluoride

377 membrane (PVDF; 0.2 μm, Bio-Rad) using a 96-well vacuum dot-blotter (Bio-Rad). The
378 membrane was then washed thrice with PBS, blocked with 5% skim milk for 30 min, and
379 subjected to a one-step immuno-affinity reaction using the rabbit peroxidase-anti-peroxidase
380 soluble complex antibody (Sigma-Aldrich, St. Louis, USA). The membrane was developed,
381 and bound antibodies were detected by chemiluminescence.
382
383 **Treatment of rice leaf extract for proteome analysis**
384 *Oryza sativa* L. cv. Milyang 23, a Xoo-susceptible rice cultivar, was used for performing
385 proteome analysis. Rice plants were grown in a paddy field at Jeonju in South Korea
386 (35°49'52.0"N 127°03'55.6"E) until panicle initiation (approximately 8 to 9 weeks). Forty
387 clumped rice leaves were harvested and homogenized with liquid nitrogen using a mortar and
388 pestle. One-gram aliquots of the resulting homogenate (RLX) were transferred to Eppendorf
389 tubes and stored at -80°C. Xoo was cultured (100 mL) in nutrient broth up to the mid-
390 exponential phase ($A_{600} = 0.5$) in a shaking incubator at 28°C and 200 rpm, and RLX (2 g) was
391 then added to the culture medium. The culture (100 mL) was subjected to sequential filtration
392 through a gauze, 40-μm nylon cell strainer (FALON, New York, USA), and 5-μm syringe filter
393 (Sartorius, Germany) to remove RLX (0, 30, 60, 90, and 120 min after RLX addition). The
394 filtered culture (100 mL) was centrifuged at 10,000 ×*g* and 4°C for 10 min. Duplicate samples
395 were obtained for each time point from two independent experiments.
396
397 **Sample preparation for proteome analysis**
398 The harvested samples were lysed in a lysis buffer (9 M urea prepared in 20 mM HEPES (pH
399 7.5), supplemented with protease inhibitor cocktail (Complete mini, Roche) and phosphatase
400 inhibitor (PhosSTOP, Sigma-Aldrich)) and sonicated on ice. The exact amount of proteins in

each sample was determined using the bicinchoninic acid assay. Protein integrity was confirmed by SDS-PAGE and 200 µg of protein from each sample was used for analysis. The disulfide bonds were reduced by treatment with 10 mM dithiothreitol for 1 h, and incubation with 30 mM iodoacetamide (30 min in the dark) was performed to alkylate free sulfhydryl functional groups. Samples were diluted with triethylammonium bicarbonate buffer (pH 8.0) in a manner such that the final urea concentration was 1.5 M. Proteins were digested using MS grade trypsin (Thermo Fisher Scientific) at a protein to enzyme ratio of 50:1 for 12 h at 37°C. The reaction was quenched by lowering the sample pH (<3) using trifluoroacetic acid. The obtained peptides were desalted using a C18 spin column (Harvard) to remove salts and other contaminants, and the purified peptides were dried. Then, they were isotopically labeled using the 10-plex tandem mass tag (TMT, Thermo Fisher Scientific), as per the manufacturer's protocol. The reaction was allowed to continue for 2 h at room temperature and TMT-labeled samples were subsequently dried in a SpeedVac concentrator. Chemical labeling with TMT was confirmed by liquid chromatography-tandem mass spectrometry (LC-MS/MS), and the samples were pooled and fractionated using a basic reverse phase liquid chromatography (RPLC) system. The pooled TMT-labeled peptide mixture was resuspended in 10 mM ammonium formate and fractionated into 12 fractions using a C18 column (C_{18}, 5 µm pore size, 4.6 mm × 250 mm, XBridge, Waters). The fractionated peptides were dried and stored at -80°C until LC-MS/MS analysis.

LC-MS/MS and database search

Each fractionated peptide sample was analyzed using an Orbitrap Fusion™ Lumos™ Tribrid™ Mass Spectrometer coupled with the Easy-nLC 1200 nano-flow liquid chromatography system (Thermo Fisher Scientific). The dried peptides were reconstituted using 0.1% formic acid and

425 loaded on a C18 trap column. Peptides were resolved using a linear gradient solvent B (0.1%
426 formic acid in 95% acetonitrile) and analyzed by high resolution mass spectrometry in the data-
427 dependent acquisition mode. MS1 and MS2 were acquired for the precursor and the peptide
428 fragmentation ions, respectively. MS1 scans were measured at a resolution of 120,000 and
429 an *m/z* of 200. MS2 scans were acquired following the fragmentation of precursor ions by high-
430 energy collisional dissociation (HCD) and were detected at a mass resolution of 50,000 and
431 an *m/z* of 200. Dynamic exclusion was used to reduce redundant fragmentation of the same
432 ions. The obtained mass spectrometry data were analyzed using the MaxQuant software
433 (Tyanova, Temu, & Cox, 2016). Raw MS data were searched against the Xoo proteome in
434 UniProt database. Carbamidomethylation of cysteine and 10-plex TMT modification of lysine
435 and N-terminals were set as static modifications, whereas oxidation of methionine was set as a
436 variable modification. False discovery rates at the levels of protein and peptide-spectrum
437 matches were set at 0.01. The raw MS data and MaxQuant search results have been submitted
438 to ProteomeXchange (project accession: PXD020135, reviewer access
439 with username: reviewer34070@ebi.ac.uk and password: mzn76I1O).
440
441 **Proteomic data analysis**
442 The contaminant and reverse identified proteins were removed from the MaxQuant data.
443 Proteins identified in both replicates were pooled for quantile normalization. The normalized
444 values for the replicates were subjected to supervised hierarchical clustering and principal
445 component analysis, using Perseus (Tyanova, Temu, Sinitcyn, et al., 2016), and the results were
446 depicted in the form of a multi-scatter plot.
447
448 **STRING map analysis**

449 The list of proteins in the selected patterns from the hierarchical clusters was uploaded on the
450 STRING database (https://string-db.org/) to analyze the protein interaction maps. The clusters
451 of proteins in the blue and red classes, which show the similar time-resolved expression
452 patterns, were analyzed, and the list including the gene names with the selected organism was
453 inputted in the multiple proteins search setting. The number of nodes and edges were
454 automatically calculated based on Xoo genes with a PPI enrichment p-value of 20.9E-10.
455 Figures were downloaded in the PNG file format for visualization.
456

457 **RNA-Seq and data analysis**

458 In addition to the previously obtained RNA-Seq data for P-activated Xoo cells, RNA-Seq data
459 at 90 and 120 min were obtained to correspond with the proteome data at these time points.
460 RNA-Seq and data analysis were performed as previously described (S. Kim et al., 2016).
461 Briefly, total RNA from samples was used to generate sequencing libraries, from which
462 ribosomal RNA was removed using MICROBExpress Bacterial mRNA Enrichment Kit
463 (Ambion, Austin, TX, USA), and enriched mRNA was prepared using Illumina TruSeq RNA
464 Sample Preparation Kit (Illumina, San Diego, CA, USA). The RNA obtained after
465 fragmentation was used to generate cDNA fragments, which were sequenced using Illumina
466 Genome Analyzer IIx and mapped to the reference genome sequence
467 (http://www.ncbi.nlm.nih.gov/nuccore/58579623?report=fasta) using CLC Genomics
468 Workbench 4.0 (CLC bio, Aarhus, Denmark). Relative transcript abundance was calculated
469 based on the number of reads per kilobase per million mapped sequence reads (RPKM).
470

471 **Analysis of time-resolved continuous mRNA and protein expression**

472 The RPKM values of the mRNAs in the transcriptome and TMT intensities of the proteins

473 in the proteome corresponded to the observed expression level of each gene at a given time
474 point. To facilitate the comparison of gene expression levels, the observed expression level at
475 each time point was converted to fold change in gene expression, by dividing the expression
476 level at a given time point by the initial expression level (0 min) of the same gene. The fold
477 change in the time-resolved expression levels of a given gene during the two hours following
478 the RLX treatment was fitted to a curve and analyzed using non-linear regression by GraphPad
479 Prism (version 3.02 for Windows, GraphPad Software, San Diego California USA,
480 www.graphpad.com), and the continuous time-dependent changes in the mRNA and protein
481 expression levels were determined using the fitted curve.
482
483 **Analysis of the correspondence between mRNA and protein expression levels**
484 For the accurate comparison of the mRNA and protein expression levels in P-activated Xoo
485 cells, the expression levels were corrected by comparing with those in the control cells at each
486 time point. The fold change in mRNA and protein expression in P-activated Xoo cells at a given
487 time point was divided by that of the control cells at the same time point. For analyzing the
488 correspondence between the mRNA and protein levels of each gene in the transcriptome and
489 proteome, the resulting control-corrected fold change values of mRNAs were compared with
490 those of the proteins for a given time point as the gene expression level of mRNAs and proteins.
491

Declarations

Competing interests

Seunghwan Kim, Wooyoung Eric Jang, Min-Sik Kim, Jeong-Gu Kim, and Lin-Woo Kang declare that they have no conflict of interest. The authors declare no competing financial interests. This article does not contain any studies with human or animal subjects performed by the any of the authors.

Available data and material

The raw MS data and MaxQuant search results are available at ProteomeXchange (Project accession: PXD020135, Reviewer access with username: reviewer34070@ebi.ac.uk and password: mzn76I1O)

Funding

This work was undertaken in association with the Cooperative Research Program for Agriculture Science & Technology Development (Project No. PJ01327002020), Rural Development Administration, Republic of Korea.

Author Contributions

Investigation, Seunghwan Kim, Wooyoung Eric Jang, Min-Sik Kim, Jeong-Gu Kim, and Lin-Woo Kang; writing, Seunghwan Kim, Wooyoung Eric Jang, Min-Sik Kim, Jeong-Gu Kim, and Lin-Woo Kang; methodology, Seunghwan Kim, Wooyoung Eric Jang, Min-Sik Kim, Jeong-Gu Kim, and Lin-Woo Kang; funding acquisition, Jeong-Gu Kim, and Lin-Woo Kang; supervision, Min-Sik Kim, Jeong-Gu Kim, and Lin-Woo Kang. All authors have read and

agreed to the published version of the manuscript.

Acknowledgments

This study was supported by the Cooperative Research Program for Agriculture Science & Technology Development (Project No. PJ01327002020), Rural Development Administration and by the 2021 RDA Fellowship Program of National Institute of Agricultural Sciences, Rural Development Administration, Republic of Korea.

Abbreviations

Xoo, *Xanthomonas oryzae* pv. *oryzae*; RLX, rice leaf homogenate; KACC, Korean Agricultural Collection Center; P-activated, Pathogenicity-activated; LC-MS/MS, liquid chromatography-tandem mass spectrometry; COG, Clusters of Orthologous Groups; RPKM, Reads per kilobase per million mapped reads

References

Garau, G., Garcia-Saez, I., Bebrone, C., Anne, C., Mercuri, P., Galleni, M., . . . Dideberg, O. (2004). Update of the standard numbering scheme for class B beta-lactamases. *Antimicrob Agents Chemother, 48*(7), 2347-2349. doi: 10.1128/AAC.48.7.2347-2349.2004

Hershey, J. W. B., Sonenberg, N., & Mathews, M. B. (2019). Principles of Translational Control. *Cold Spring Harb Perspect Biol, 11*(9). doi: 10.1101/cshperspect.a032607

Jackson, S. A. (2016). Rice: The First Crop Genome. *Rice (N Y), 9*(1), 14. doi: 10.1186/s12284-016-0087-4

Jones, J. D., & Dangl, J. L. (2006). The plant immune system. *Nature, 444*(7117), 323-329. doi: 10.1038/nature05286

Kay, S., Hahn, S., Marois, E., Wieduwild, R., & Bonas, U. (2009). Detailed analysis of the DNA recognition motifs of the Xanthomonas type III effectors AvrBs3 and AvrBs3Deltarep16. *Plant J, 59*(6), 859-871. doi: 10.1111/j.1365-313X.2009.03922.x

Kim, S., Cho, Y. J., Song, E. S., Lee, S. H., Kim, J. G., & Kang, L. W. (2016). Time-resolved pathogenic gene expression analysis of the plant pathogen Xanthomonas oryzae pv. oryzae. *BMC Genomics, 17*, 345. doi: 10.1186/s12864-016-2657-7

Kim, S. H., Lee, S. E., Hong, M. K., Song, N. H., Yoon, B., Viet, P., . . . Kang, L. W. (2011). Homologous expression and quantitative analysis of T3SS-dependent secretion of TAP-tagged XoAvrBs2 in Xanthomonas oryzae pv. oryzae induced by rice leaf extract. *J Microbiol Biotechnol, 21*(7), 679-685.

Kim, S., Nguyen, T. D., Lee, J., Hong, M. K., Pham, T. V., Ahn, Y. J., . . . Kang, L. W. (2013). Homologous expression and T3SS-dependent secretion of TAP-tagged Xo2276 in Xanthomonas oryzae pv. oryzae induced by rice leaf extract and its direct in vitro recognition of putative target DNA sequence. *J Microbiol Biotechnol, 23*(1), 22-28.

Lee, B. M., Park, Y. J., Park, D. S., Kang, H. W., Kim, J. G., Song, E. S., . . . Go, S. J. (2005). The genome sequence of Xanthomonas oryzae pathovar oryzae KACC10331, the bacterial blight pathogen of rice. *Nucleic Acids Res, 33*(2), 577-586. doi: 10.1093/nar/gki206

Li, J. Y., Wang, J., & Zeigler, R. S. (2014). The 3,000 rice genomes project: new opportunities and challenges for future rice research. *Gigascience, 3*, 8. doi: 10.1186/2047-217X-3-8

Liu, Y., Kong, D., Wu, H. L., & Ling, H. Q. (2020). Iron in Plant-pathogen Interactions. *J Exp Bot*. doi: 10.1093/jxb/eraa516

Mew, T. W., Alvarez, A. M., Leach, J. E., & Swings, J. (1993). Focus on Bacterial-Blight of Rice. *Plant Disease, 77*(1), 5-12. doi: Doi 10.1094/Pd-77-0005

Mukherjee, S., & Kearns, D. B. (2014). The structure and regulation of flagella in Bacillus subtilis. *Annu Rev Genet, 48*, 319-340. doi: 10.1146/annurev-genet-120213-092406

Oliva, R., Ji, C., Atienza-Grande, G., Huguet-Tapia, J. C., Perez-Quintero, A., Li, T., . . . Yang, B. (2019). Broad-spectrum resistance to bacterial blight in rice using genome editing. *Nat Biotechnol, 37*(11), 1344-1350. doi: 10.1038/s41587-019-0267-z

Quibod, I. L., Atieza-Grande, G., Oreiro, E. G., Palmos, D., Nguyen, M. H., Coronejo, S. T., . . . Oliva, R. (2020). The Green Revolution shaped the population structure of the rice pathogen Xanthomonas oryzae pv. oryzae. *ISME J, 14*(2), 492-505. doi: 10.1038/s41396-019-0545-2

Schubert, O. T., Rost, H. L., Collins, B. C., Rosenberger, G., & Aebersold, R. (2017). Quantitative proteomics: challenges and opportunities in basic and applied research. *Nat Protoc, 12*(7), 1289-1294. doi: 10.1038/nprot.2017.040

Tsuge, S., Furutani, A., & Ikawa, Y. (2014). Regulatory network of hrp gene expression in Xanthomonas oryzae pv. oryzae. *Journal of General Plant Pathology, 80*(4), 303-313. doi: 10.1007/s10327-014-0525-3

Tyanova, S., Temu, T., & Cox, J. (2016). The MaxQuant computational platform for mass spectrometry-based shotgun proteomics. *Nat Protoc, 11*(12), 2301-2319. doi: 10.1038/nprot.2016.136

Tyanova, S., Temu, T., Sinitcyn, P., Carlson, A., Hein, M. Y., Geiger, T., . . . Cox, J. (2016). The Perseus computational platform for comprehensive analysis of (prote)omics data. *Nat Methods, 13*(9), 731-740. doi: 10.1038/nmeth.3901

Ullah, J. H., Walsh, T. R., Taylor, I. A., Emery, D. C., Verma, C. S., Gamblin, S. J., & Spencer, J. (1998). The crystal structure of the L1 metallo-beta-lactamase from Stenotrophomonas maltophilia at 1.7 A resolution. *J Mol Biol, 284*(1), 125-136. doi: 10.1006/jmbi.1998.2148

596 **Scheme legend**

597

598 **Scheme 1.** Schematic representation of the in vitro assay system and combined analysis of

599 the time-resolved transcriptome and proteome using RNA-Seq and LC-MS/MS

600

601

602 ## Figure legends

603

604 **Figure 1. Time-supervised hierarchical clustering of duplicate pathogenicity-activated**
605 **proteome datasets.** The heatmap (left) of genes clustered based on the similarities in the
606 protein expression pattern over time is presented for duplicate samples of pathogenicity-
607 activated and control Xoo cells. Low to high expression is indicated by a change in color from
608 green to red. Selected cluster profile patterns (right) are presented for the downregulated (blue
609 box) and upregulated (red box) genes in the P-activated Xoo cells.

610

611 **Figure 2. Time-resolved protein expression patterns associated with the COG categories**.
612 Two functional categories of genes (COG) associated with the greatest changes in the protein
613 level are indicated by red boxes, nine functional COGs associated with moderate changes are
614 indicated by yellow boxes, and other nine functional COGs associated with minor changes in
615 the protein level are indicated by blue boxes. The inset for each functional COG indicates the
616 control (untreated cells). The Y-axis represents the fold change in the protein expression level
617 in comparison with that at 0 min, and the maximum value on the Y-axis was set as 3. The X-
618 axis indicates the time from 0 to 120 min. Each line indicates the protein expression level of a
619 gene. The protein expression level is represented as grey (from 0 to 30 min) and black (from
620 30 to 120 min) lines. Note that in contrast to the transcript data, the proteome data was not
621 available between 0 and 30 min (grey part).

622

623 **Figure 3. Time-resolved mRNA and protein levels of genes associated with cell motility**
624 **and inorganic ion transport.** (A) Time-resolved expression of cell motility-related genes. The
625 mRNA expression levels from RNA-Seq are indicated by dashed red lines. The protein

626 expression levels from LC-MS/MS are indicated by black dashed (from 0 to 30 min) and black
627 solid (from 30 to 120 min) lines. (B) Time-resolved expression of inorganic ion transport-
628 related genes. The mRNA expression levels from RNA-Seq and protein expression levels from
629 LC-MS/MS are indicated as in (A). The Y-axis represents the fold change.
630
631 **Figure 4. Gene clusters and time-resolved expression patterns of cell motility-related**
632 **genes.** (A) Gene clusters of flagellar biosynthesis-related genes (groups I-A and I-B) and
633 chemotaxis genes (group II). (B) Time-resolved mRNA and protein expression levels of genes
634 in groups I-A, I-B, and II. The down- and upregulation peaks are shown in green and red,
635 respectively. The yellow and grey ovals indicate unaltered and undetected expression levels.
636 The thin-bordered oval (at 5, 10, 15, and 45 min) for the proteome data is to ensure consistency
637 with the pictorial format of RNA-Seq data. The dotted arrows and ovals indicate genes that are
638 not directly related to flagellar biosynthesis and chemotaxis. Time is expressed in min.
639
640 **Figure 5. Time-resolved mRNA and protein levels of iron transport-related genes.** (A)
641 Time-resolved mRNA (red) and protein (black) expression levels of *FecA* and *CirA* genes. (B)
642 Time-resolved mRNA (red) and protein (black) expression level of *IroN* genes. The Y-axis
643 represents $\log_2$(fold-change).
644
645 **Figure 6. Time-resolved mRNA and protein expression and secretion of effector proteins.**
646 The mRNA (red) and protein (black) expression levels of *XoAvrBs2* (A) and *XoAvrBs3* (B)
647 genes in the transcriptome and proteome data (above) and the cytosolic and secreted XoAvrBs2
648 (A) and XoAvrBs3 (B) proteins in the dot blot data (below). NC, negative control; PC, positive
649 control

650

651 **Figure 7. Schematic representation of genome-wide pathogenic gene expression and**
652 **effector secretion via in vitro assay system.** Early response Xoo genes from the initial
653 interaction with RLX include genes related to cell motility, iron uptake, and effector, of which
654 expression are upregulated as early as 5 min in mRNAs and 30 min in proteins and effector
655 secretion is found since 15 min.

656

Scheme 1

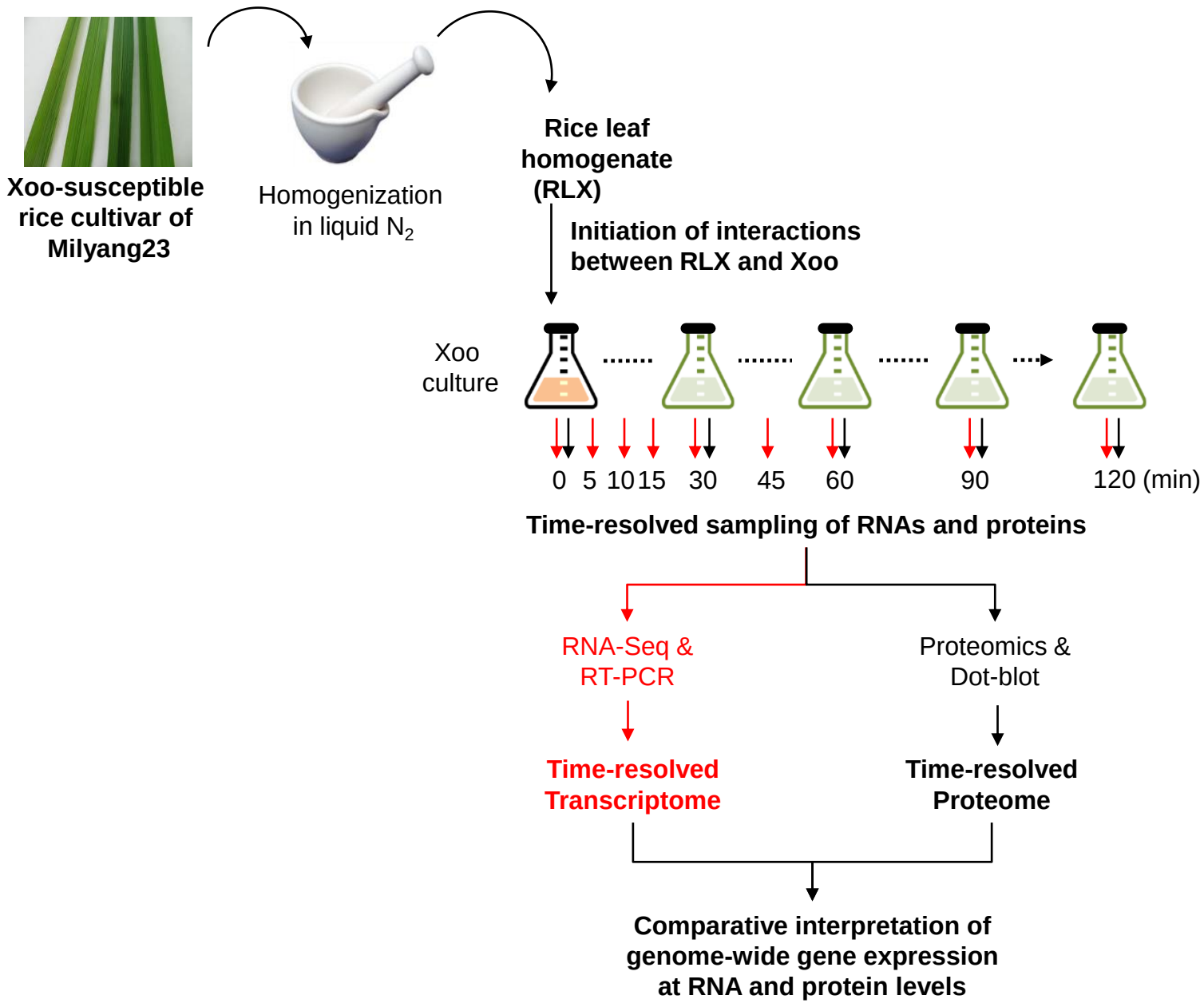
Xoo-susceptible rice cultivar of Milyang23
Homogenization in liquid N_2
Rice leaf homogenate (RLX)
Initiation of interactions between RLX and Xoo
Xoo culture
0 5 10 15 30 45 60 90 120 (min)
Time-resolved sampling of RNAs and proteins
RNA-Seq & RT-PCR
Proteomics & Dot-blot
Time-resolved Transcriptome
Time-resolved Proteome
Comparative interpretation of genome-wide gene expression at RNA and protein levels

Figure 1

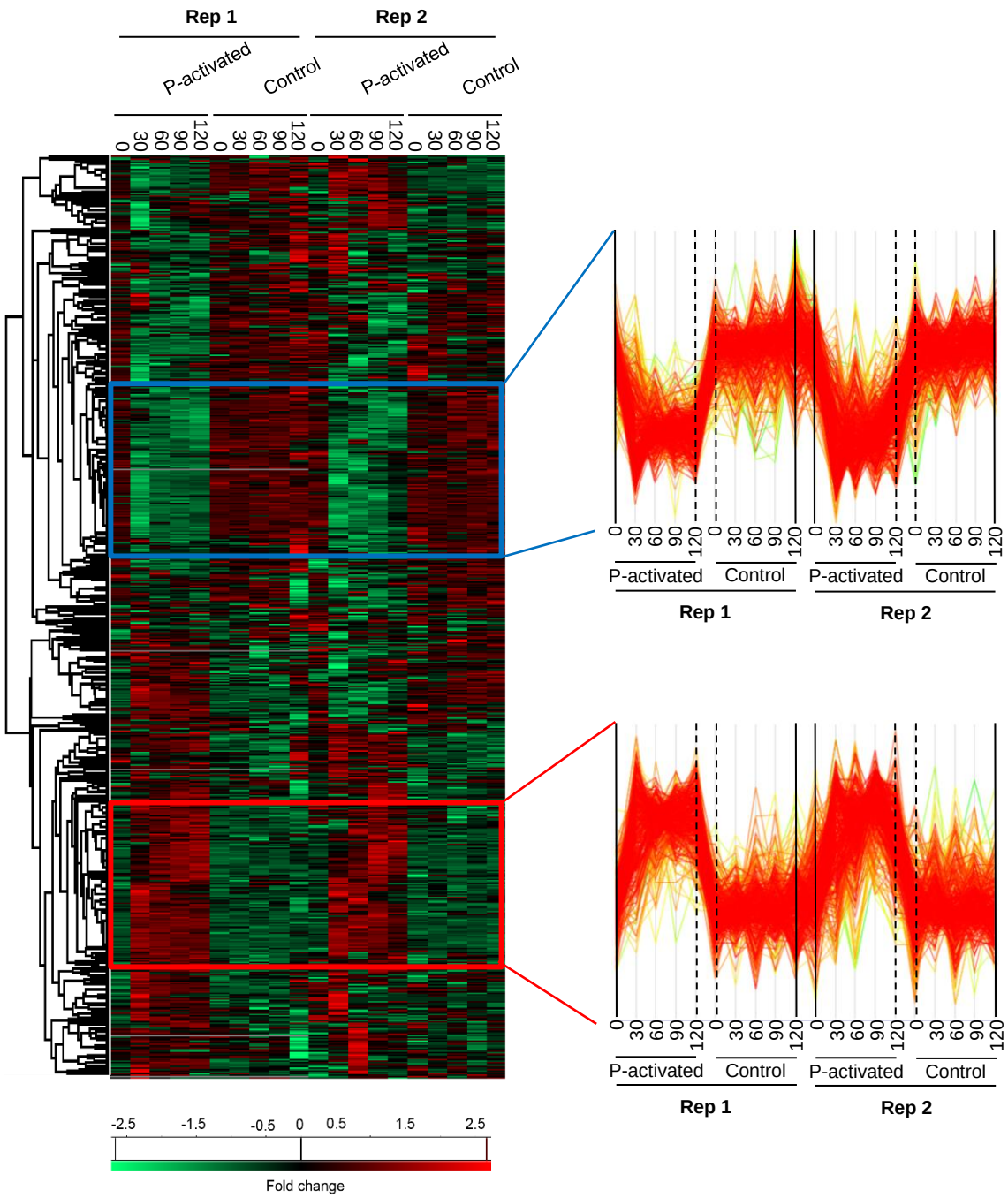
Rep 1
Rep 2
P-activated
Control
P-activated
Control
0
30
60
90
120
-2.5
-1.5
-0.5
0
0.5
1.5
2.5
Fold change
P-activated
Control
P-activated
Control
Rep 1
Rep 2
P-activated
Control
P-activated
Control
Rep 1
Rep 2

Figure 2

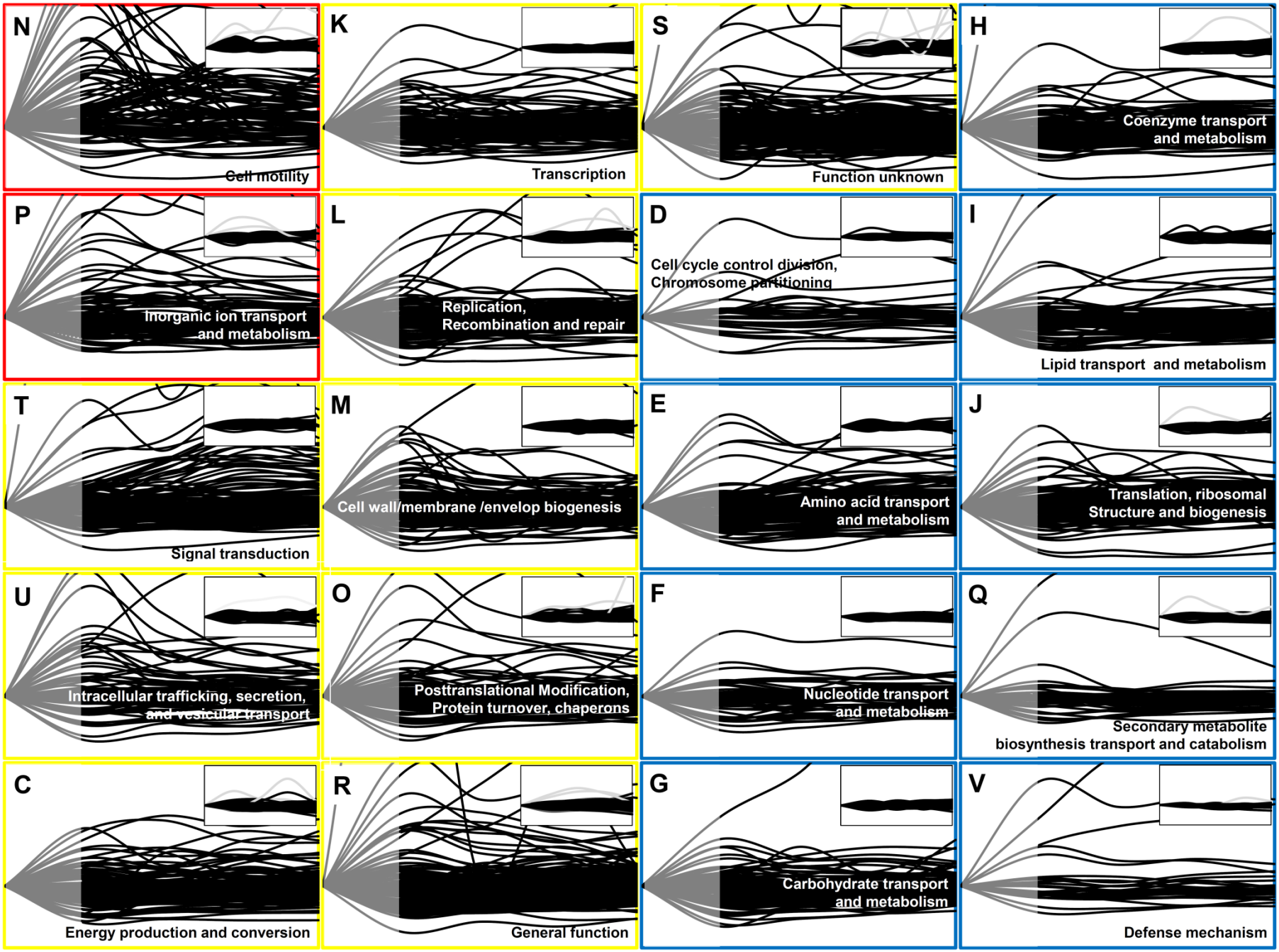
N
Cell motility
K
Transcription
S
Function unknown
H
Coenzyme transport
and metabolism
P
Inorganic ion transport
and metabolism
L
Replication,
Recombination and repair
D
Cell cycle control division,
Chromosome partitioning
I
Lipid transport and metabolism
T
Signal transduction
M
Cell wall/membrane /envelop biogenesis
E
Amino acid transport
and metabolism
J
Translation, ribosomal
Structure and biogenesis
U
Intracellular trafficking, secretion,
and vesicular transport
O
Posttranslational Modification,
Protein turnover, chaperons
F
Nucleotide transport
and metabolism
Q
Secondary metabolite
biosynthesis transport and catabolism
C
Energy production and conversion
R
General function
G
Carbohydrate transport
and metabolism
V
Defense mechanism

Figure 3

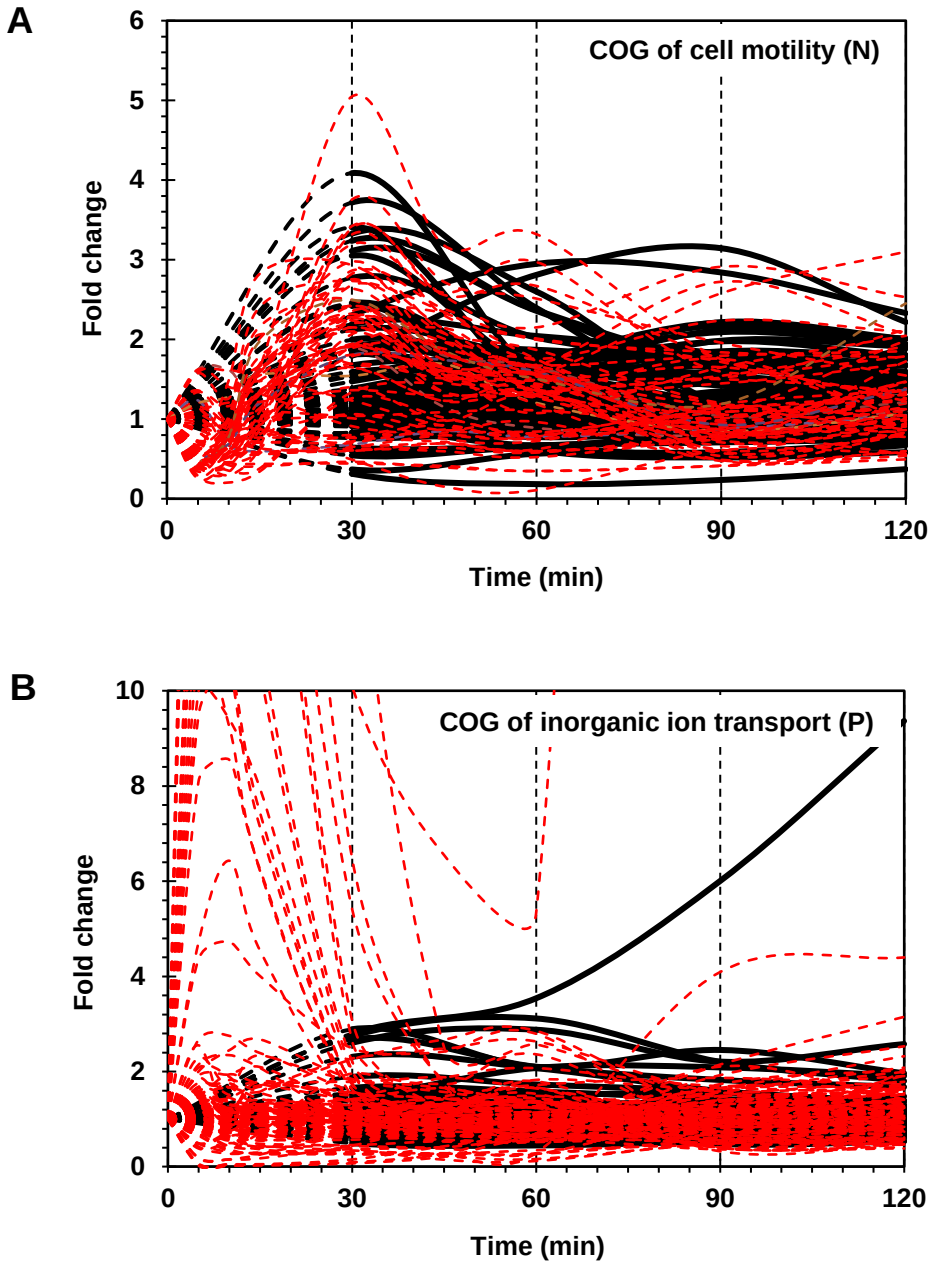
A
COG of cell motility (N)
Fold change
Time (min)
0
1
2
3
4
5
6
0
30
60
90
120
B
COG of inorganic ion transport (P)
Fold change
Time (min)
0
2
4
6
8
10
0
30
60
90
120

Figure 4

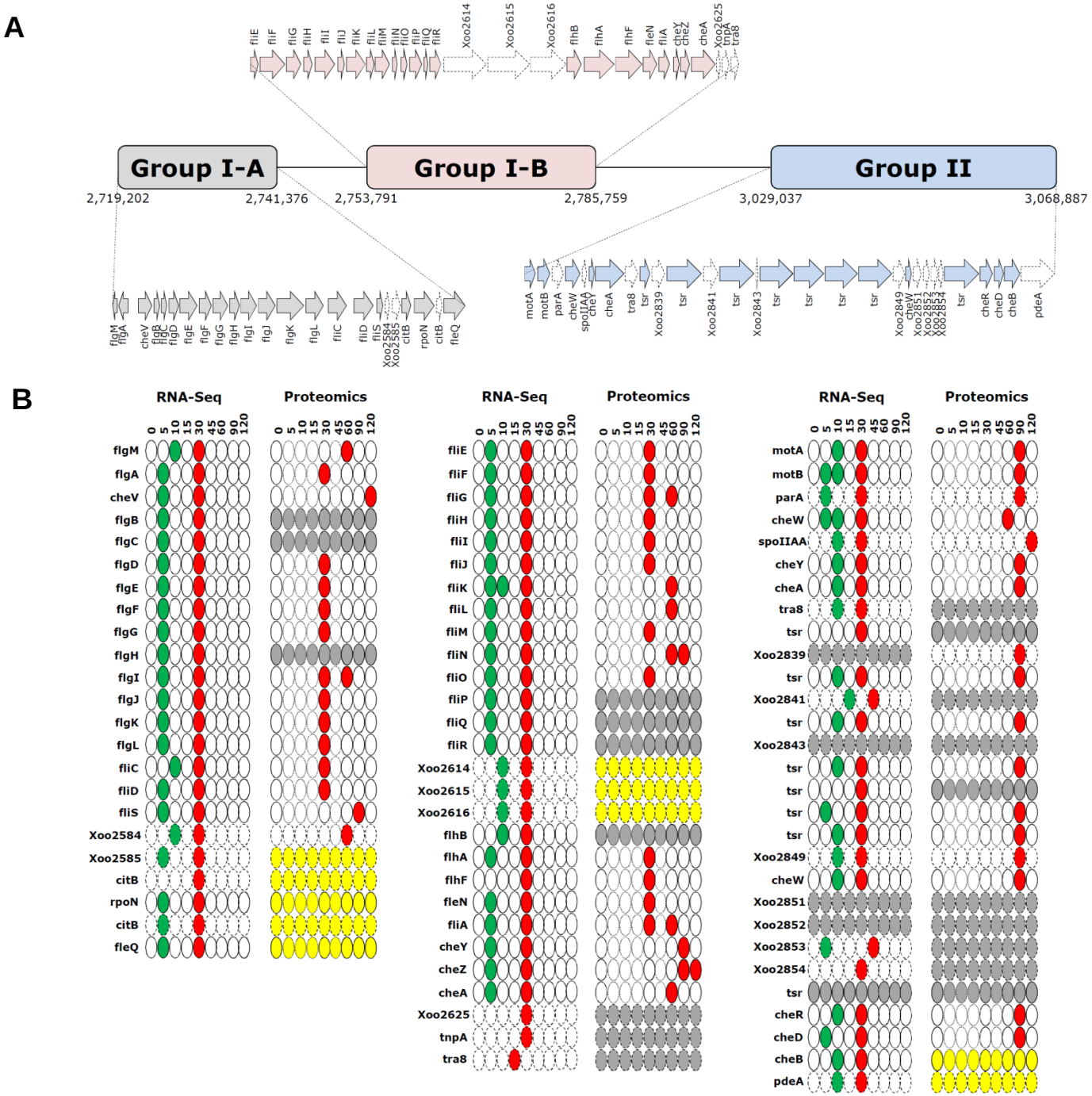
A
Group I-A
Group I-B
Group II
2,719,202
2,741,376
2,753,791
2,785,759
3,029,037
3,068,887
B
RNA-Seq
Proteomics
0 5 10 15 30 45 60 90 120
flgM
flgA
cheV
flgB
flgC
flgD
flgE
flgF
flgG
flgH
flgI
flgJ
flgK
flgL
fliC
fliD
fliS
Xoo2584
Xoo2585
citB
rpoN
citB
fleQ
fliE
fliF
fliG
fliH
fliI
fliJ
fliK
fliL
fliM
fliN
fliO
fliP
fliQ
fliR
Xoo2614
Xoo2615
Xoo2616
flhB
flhA
flhF
fleN
fliA
cheY
cheZ
cheA
Xoo2625
tnpA
tra8
motA
motB
parA
cheW
spoIIAA
cheY
cheA
tra8
tsr
Xoo2839
tsr
Xoo2841
tsr
Xoo2843
tsr
tsr
tsr
tsr
Xoo2849
cheW
Xoo2851
Xoo2852
Xoo2853
Xoo2854
tsr
cheR
cheD
cheB
pdeA

Figure 5

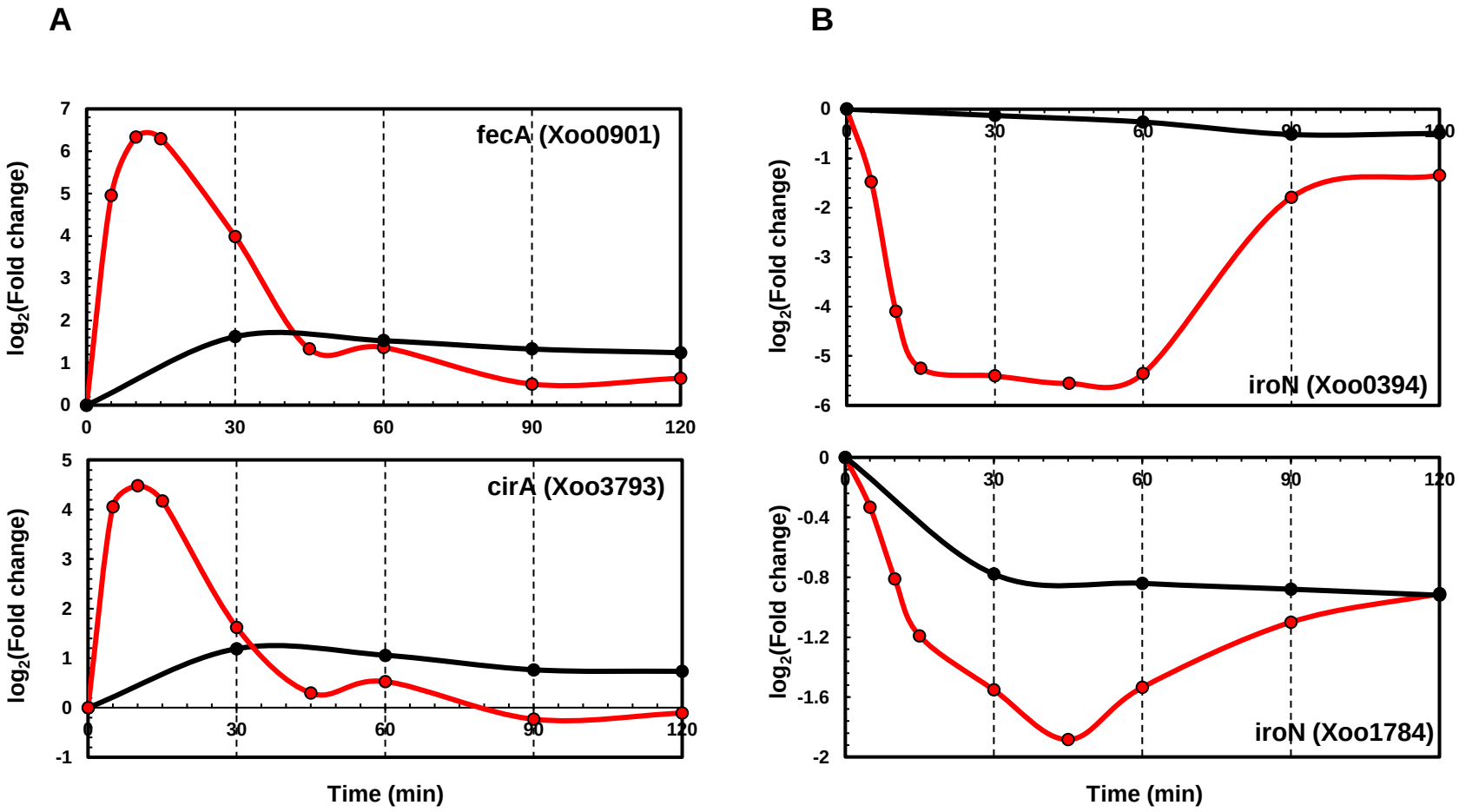
A
B
fecA (Xoo0901)
cirA (Xoo3793)
iroN (Xoo0394)
iroN (Xoo1784)
log2(Fold change)
Time (min)
0
30
60
90
120
7
6
5
4
3
2
1
0
-1
-2
-3
-4
-5
-6
-0.4
-0.8
-1.2
-1.6

Figure 6

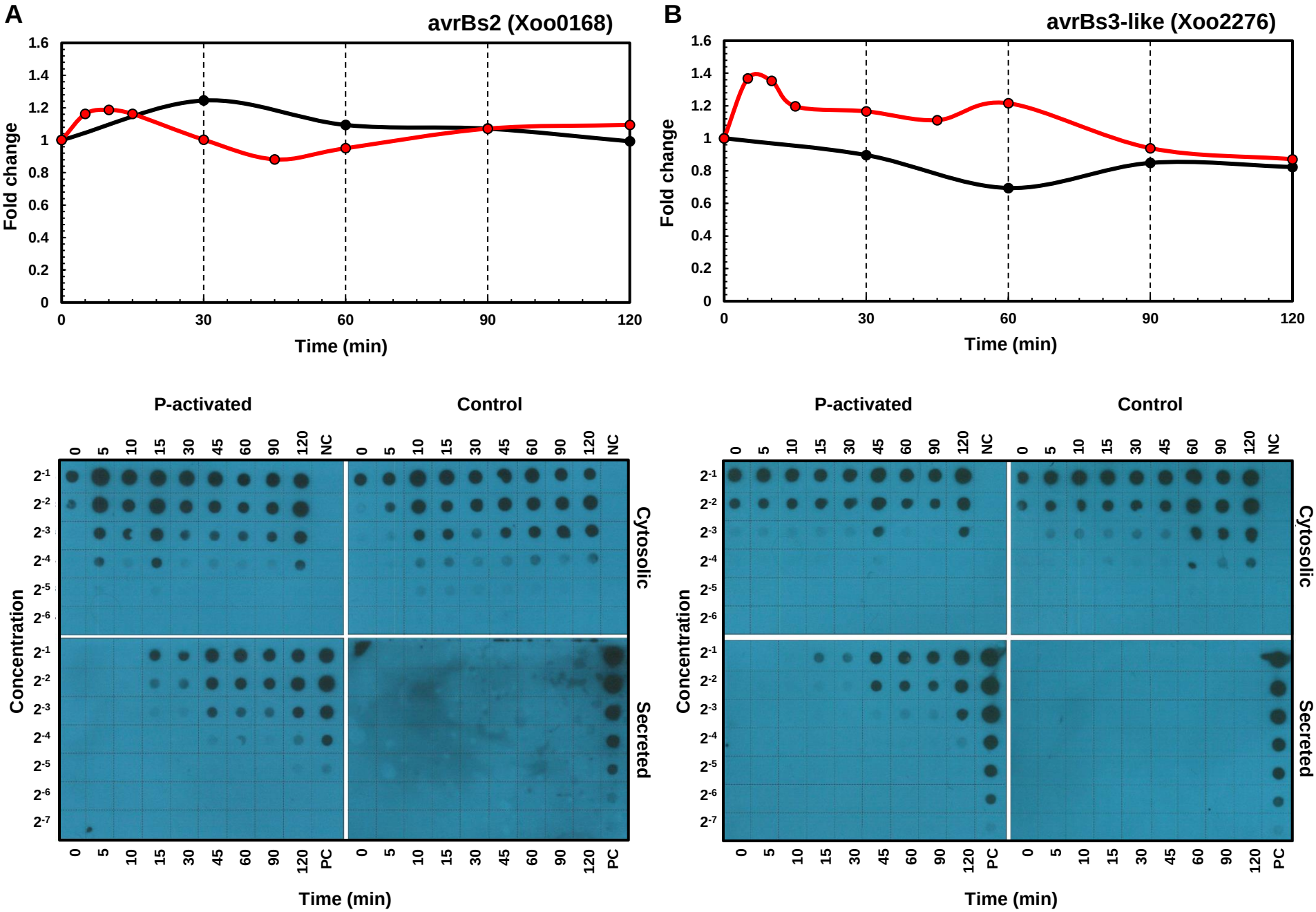
A
avrBs2 (Xoo0168)
Fold change
Time (min)
B
avrBs3-like (Xoo2276)
Fold change
Time (min)
P-activated
Control
Cytosolic
Secreted
Concentration
Time (min)
P-activated
Control
Cytosolic
Secreted
Concentration
Time (min)

Figure 7

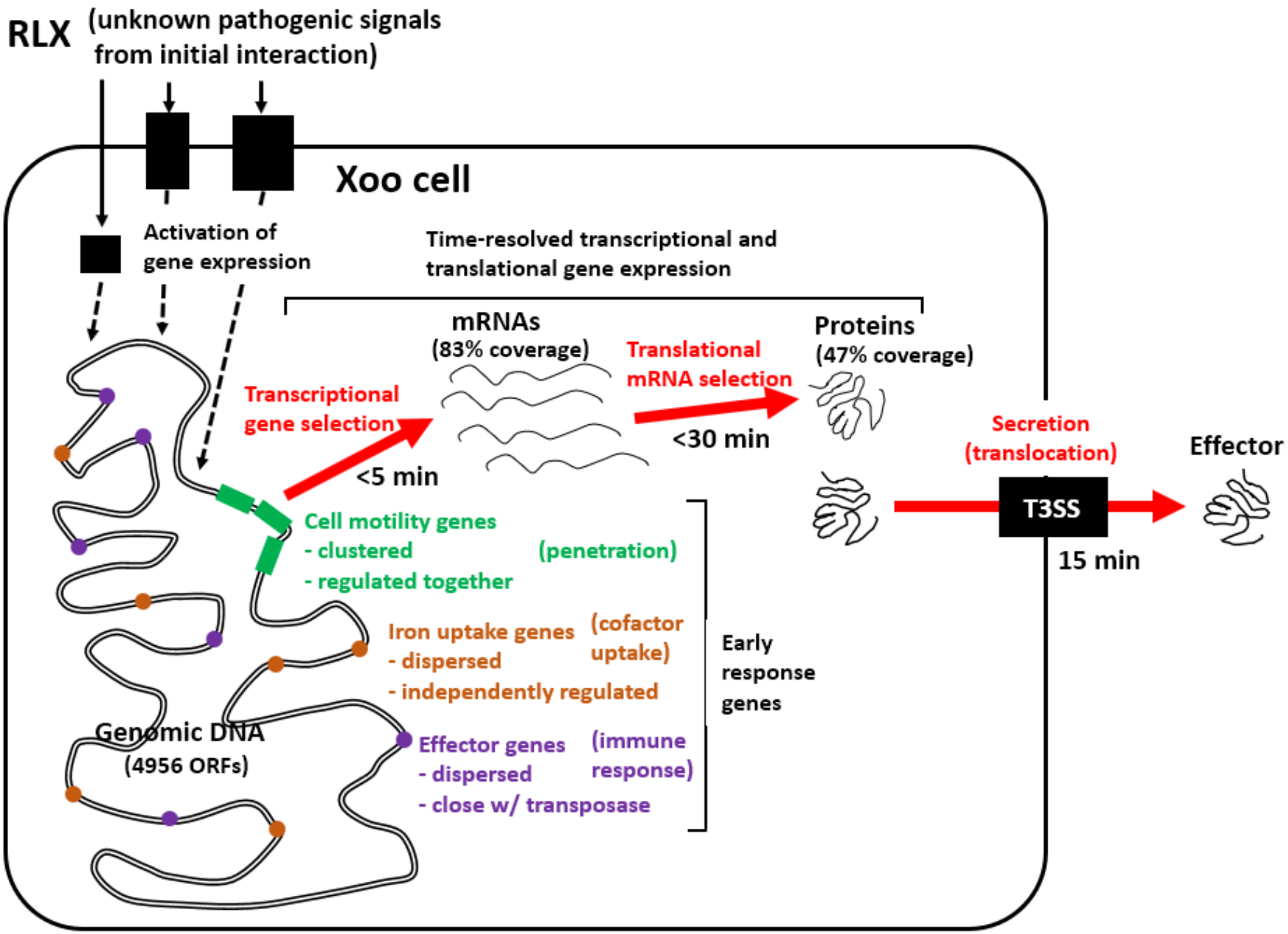
RLX
(unknown pathogenic signals from initial interaction)
Xoo cell
Activation of gene expression
Time-resolved transcriptional and translational gene expression
mRNAs
(83% coverage)
Proteins
(47% coverage)
Translational mRNA selection
Transcriptional gene selection
<30 min
<5 min
Secretion (translocation)
Effector
T3SS
15 min
Cell motility genes
- clustered
- regulated together
(penetration)
Iron uptake genes
- dispersed
- independently regulated
(cofactor uptake)
Early response genes
Genomic DNA
(4956 ORFs)
Effector genes
- dispersed
- close w/ transposase
(immune response)